



City Research Online

City, University of London Institutional Repository

Citation: Azizi, M., Talatahari, S. & Giaralis, A. (2021). Active Vibration Control of Seismically Excited Building Structures by Upgraded Grey Wolf Optimizer. *IEEE Access*, 9, pp. 166658-166673. doi: 10.1109/access.2021.3134202

This is the published version of the paper.

This version of the publication may differ from the final published version.

Permanent repository link: <https://openaccess.city.ac.uk/id/eprint/27259/>

Link to published version: <https://doi.org/10.1109/access.2021.3134202>

Copyright: City Research Online aims to make research outputs of City, University of London available to a wider audience. Copyright and Moral Rights remain with the author(s) and/or copyright holders. URLs from City Research Online may be freely distributed and linked to.

Reuse: Copies of full items can be used for personal research or study, educational, or not-for-profit purposes without prior permission or charge. Provided that the authors, title and full bibliographic details are credited, a hyperlink and/or URL is given for the original metadata page and the content is not changed in any way.

City Research Online:

<http://openaccess.city.ac.uk/>

publications@city.ac.uk

Received, accepted, date of publication, date of current version.

Digital Object Identifier

Active Vibration Control of Seismically Excited Building Structures by Upgraded Grey Wolf Optimizer

MAHDI AZIZI¹, SIAMAK TALATAHARI^{1,2}, AND AGATHOKLIS GIARALIS³

¹Department of Civil Engineering, University of Tabriz, Tabriz 5166616471, Iran

²Faculty of Engineering, Near East University, 99150 Nicosia, Turkey

³Department of Civil Engineering, City, University of London, London EC1V 0HB, U.K.

Corresponding author: Agathoklis Giaralis (agathoklis.giaralis.1@city.ac.uk)

This work was supported by the Engineering and Physical Sciences Research Council (EPSRC), U.K., under Grant EP/M017621/1. The work of Mahdi Azizi and Siamak Talatahari was supported by a research grant of the Iran National Science Foundation (INSF) under Grant 99011998.

ABSTRACT In recent decades, active vibration control of buildings for earthquake-induced damage mitigation has been widely considered in the scientific literature. Fuzzy logic control (FLC) has been shown to be an effective approach to regulate control forces exerted by actuators to building structures to reduce earthquake-borne oscillations. In many cases, FLC definition relying solely on expert knowledge does not result in optimal control responses for structures under strong ground motions. Thus, FLC optimal design becomes critical. In this regard, this paper puts forth an enhanced version of the metaheuristic Grey Wolf Optimizer (UGWO) to optimally design membership functions and rule base of FLC to minimize seismic structural damage defined in terms of maximum curvature ductility ratio at the end of structural members. The potential of UGWO for the purpose is demonstrated by considering a FLC implemented to control the seismic response of a 20-story steel structure with nonlinear behavior through active actuators. The performance of the UGWO is gauged by examining nine different structural performance metrics and compared to results from 5 different widely used state-of-art metaheuristic optimization algorithms including the original Grey Wolf Optimizer. Comparisons demonstrate the capability of UGWO in providing better solutions in most of cases, resulting in reduced structural response and damage of the considered building.

INDEX TERMS Ground motion; Fuzzy logic controller; Optimization; Upgraded Grey Wolf Optimizer; Metaheuristic.

I. INTRODUCTION

High-rise slender buildings are increasingly dominating the skyline of modern cities, making efficient use of the evermore scarce and high-premium urban land [1]. However, these structures may be susceptible to wide-band earthquake-induced lateral loads, especially in high seismicity regions [2]. To this end, active vibration control approaches have been widely pursued in the scientific literature for suppressing earthquake-borne lateral oscillations in high-rise buildings [3], aiming to increase community resilience to the seismic hazard. Such approaches employ large-scale actuators to exert time-

varying control forces to buildings such that seismic structural demands, namely lateral relative inter-storey displacements (storey drifts) and floor accelerations, are minimized. The required control forces are determined by closed-loop optimal feedback control algorithms, informed by real-time measurements of structural responses and ground motion excitation. Despite promising theoretical studies, active control technology found little practical application, compared to passive control solutions, for the seismic protection of buildings. This is mostly due to the large external energy typically required to generate the desired control forces, the cost of equipment (i.e. sensors

and actuators), and the complexity and efficiency of active controllers [4]. Nevertheless, the additive cost of active seismic control is expected to reduce in the foreseeable future with the increased availability of seismic ground motion and structural response data collected in real-time by early warning systems [5] and structural health monitoring sensor networks [6], deployed for seismic risk mitigation in smart cities [7]. Further, the efficacy and adaptiveness of active motion control over passive control solutions has been successfully demonstrated in mitigating wind-borne oscillations in real-life tall slender buildings [8]. Given that wind excitations are most critical to the design of typical tall slender buildings [9], the catalyst for extending the applicability of active control to address seismic loads in such structures is the development of more efficient active controllers tailored to minimize seismic structural demands.

To this end, this paper focuses on the development of an improved metaheuristic optimization algorithm to design a fuzzy logic controller (FLC) for efficient seismic protection of tall buildings via active control. Note that FLCs have been widely considered in the literature for active vibration control of civil structures for several years and proved their effectiveness over alternative controllers [3,10-13]. Further, there is rich literature on the use of metaheuristic optimization algorithms for FLC design in various engineering applications, some of which are reviewed here. Reddy et al. [14] utilized genetic algorithms for optimal design of a nonlinear knowledge-based FLC for active control of magnetic bearings. Hein et al. [15] developed an interpretable fuzzy controller based on the Particle Swarm Optimization for automatically adjusting all controller parameters in vibration control of industrial facilities. Vanishree and Ramesh [16] utilized the Dragonfly Algorithm for optimal configuration of the Static VAR compensator developed for power transmission systems with improved voltage profile. Azizipanah-Abarghooee et al. [17] developed a fuzzy logic-based load frequency control technique utilizing the Jaya Algorithm to reduce the oscillation of system frequency. Hasanipanah et al. [18] proposed a new hybrid methodology for the optimal design of the fuzzy systems by the Imperialist Competitive Algorithm for ground vibration from blasting at mines. Boubertakh [19] proposed a method based on Ant Colony Optimization algorithm for optimal design of Fuzzy PID (FPID) controllers for single-input single-output and multiple-input multiple-output systems. Caraveo et al. [20] investigated a modification process for a bio-inspired algorithm formulated based on the bee behavior, called Bee Colony Optimization for optimal design of fuzzy controllers. Sahoo et al. [21] utilized Differential Evolution algorithm for optimization of FPID controller for load frequency nonlinear control of interconnected power systems. Debnath et al. [22] discussed the optimal

parameter configuration of the FPID controllers utilizing the Firefly Algorithm with application to the derivative filter for the frequency control with thermal non-reheat type turbine of a unified power system. Gheisarnejad [23] designed a secondary controller based on fuzzy logic for two practical models implemented in load frequency control design problem and optimized by Cuckoo Search Algorithm. Sahoo and Panda [24] utilized Grey Wolf Optimization (GWO) algorithm for optimal control and frequency regulation in power systems based on the parameter configuration of a FPID controller. Zadeh and Bathaee [25] discussed load frequency control procedures for interconnected power systems considering uncertainty considerations and nonlinear term based on FLC using Harmony Search algorithm. Olivas et al. [26] utilized Gravitational Search Algorithm for parameter adjusting of type-2 FLC.

Meanwhile, the authors developed several metaheuristic optimization algorithms and demonstrated their enhanced efficiency over alternative algorithms in solving various engineering design optimization problems including the Tribe-Charged System Search for parameter identification of nonlinear systems with large search domains [27], the Quantum-behaved Developed Swarm Optimizer for optimal design of tall buildings [28]; the Fuzzy Adaptive Charged System Search for global optimization [29]; the Chaos Game Optimization algorithm for constrained engineering design problems [30] and the Atomic Orbital Search for global optimization [31] and constraint engineering design problems [32].

Herein, the GWO introduced by Mirjalili et al. [33] is utilized for FLC optimal design for smart active motion control of slender high-rise buildings subject to severe earthquake excitations. The GWO is a metaheuristic algorithm in which the behavior of the search agents seeking the global optimal solution mimics the hunting behavior of a typical pack of grey wolves gradually encircling their prey and ultimately attacking it. The consideration of GWO for the task is prompted by its simplicity to tackle challenging engineering optimization problems and its capability of seeking the global optimal solution in a systematic manner. Further, an improved version of GWO, termed Upgraded GWO (UGWO), is proposed in this paper to achieve enhanced seismic structural performance through improved FLC optimal design. In the UGWO an estimate of the optimal solution in the search domain is re-evaluated after the position of a single agent has been updated within each iteration of the algorithm, as opposed to re-evaluating the optimal solution location after the position of all the agents have been updated (ie, at the end of each iteration) used in the standard GWO. The proposed UGWO is utilized for optimal FLC design implemented in a 20-story nonlinear steel benchmark

building [34] subject to several recorded earthquake strong ground motions. The capability and performance of the UGWO for FLC optimum design process is compared with the standard GWO alongside latest versions of popular advanced metaheuristic and classical optimization algorithms.

II. Fuzzy Logic Controller

Conventional closed-loop motion control algorithms employ a pre-specified parametric mathematical model of the dynamically excited structure we seek to control [3]. Thus, the potential of these algorithms for effective motion control relies on the accuracy of the mathematical model to represent the structure. This accuracy is naturally reduced for complex structures with uncertain properties and/or with unforeseen nonlinear response. Such is the case of building structures whose mass and stiffness properties are uncertain at the time of an earthquake and whose response to severe seismic ground excitation may become nonlinear [7]. A viable way to address this problem is to use model-free intelligent controllers such as a FLC. The latter has been shown to be quite advantageous for active seismic control of buildings as it can handle efficiently complex phenomena such as nonlinear structural seismic response due to material yielding [12,13].

In particular, a typical FLC undertakes three distinct operations. First, the FLC transcribes the input crisp data into a number of predefined linguistic arguments (fuzzy variables). This transcription operation, termed fuzzification, is based on membership functions which map input crisp data onto the fuzzy variables following fuzzy set theory. Second, inference is conducted to determine the control action in the fuzzy domain. This inference operation uses a rule base of “if-then” fuzzy logic operators, commonly specified through human expert knowledge. Third, transcription of the control action from fuzzy variables to crisp control force values takes place, termed defuzzification. The latter operation is based on membership functions, different from those used in the fuzzification operation, mapping the fuzzy control action variables onto output crisp values. A schematic view of a FLC implemented in a closed-loop control system is presented in Fig. 1 showing the sequence of the three above described operations: fuzzification, inference and defuzzification.

In the numerical part of this work, a particular FLC is adopted to regulate output active control forces for earthquake response mitigation of a building based on structural acceleration input measurements. The considered FLC is a modified version of the one proposed by Al-Dawod et al. [12]. The latter was strictly knowledge-based, relying on human expertise/intuition to define the support of membership functions and the rule base. For this reason,

the FLC was sub-optimal and its effectiveness for structural seismic response mitigation was reported to be quite limited. Here, the FLC in [12] is modified to allow for variability to the membership function support and to the rule base, through a set of different (design) variables. Then, optimization of the design variables based on seismic structural response data allows for defining an enhanced FLC which is driven by structure-specific data rather than relying solely on human knowledge.

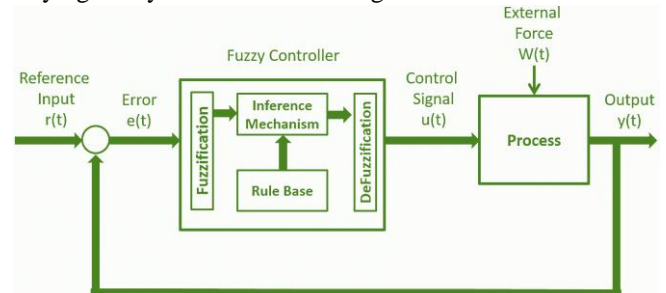


FIGURE 1. Fuzzy logic controller implemented in a closed-loop control system.

In detail, the adopted FLC considers two input data streams (building response accelerations) and one output data stream (control force). Eleven linguistic fuzzy variables are utilized to define the fuzzy domain, presented in Table 1. Eight different membership functions are used for the fuzzification of each of the input data stream and eleven membership functions for the defuzzification of the output data. Membership functions are triangularly shaped with parametrically defined support through eleven variables (a_1, a_2, \dots, a_{11}) for each input and fifteen variables (b_1, b_2, \dots, b_{15}) for the output, as shown in Fig.2.

TABLE 1. Fuzzy linguistic variables.

Variables	Definition
PVL	Positive and very Large
PL	Positive and Large
PM	Positive and Medium
PS	Positive and Small
PVS	Positive and very Small
ZR	Zero
NVS	Negative and very Small
NS	Negative and Small
NM	Negative and Medium
NL	Negative and Large
NVL	Negative and very Large

The rule base of the considered FLC comprises 64 “if-then” fuzzy rules reported in Table 2. Each rule is assigned a weight c_i ($i=1,2,\dots,64$) taking values within $[0,1]$ interval, and treated as design variable. The value of the weight c_i signifies the importance of the i th rule in the fuzzy rule base. For $c_i = 1$, the i th rule has maximum importance in

the fuzzy inference operation, while for $c_i = 0$, the i th rule does not participate in the inference. For $0 < c_i < 1$, the i th rule has a partial participation/effect in the inference operation depending on the c_i value.

In the following section metaheuristic algorithms are reviewed that will be used to optimally design the three sets of parameters defining the adopted FLC.

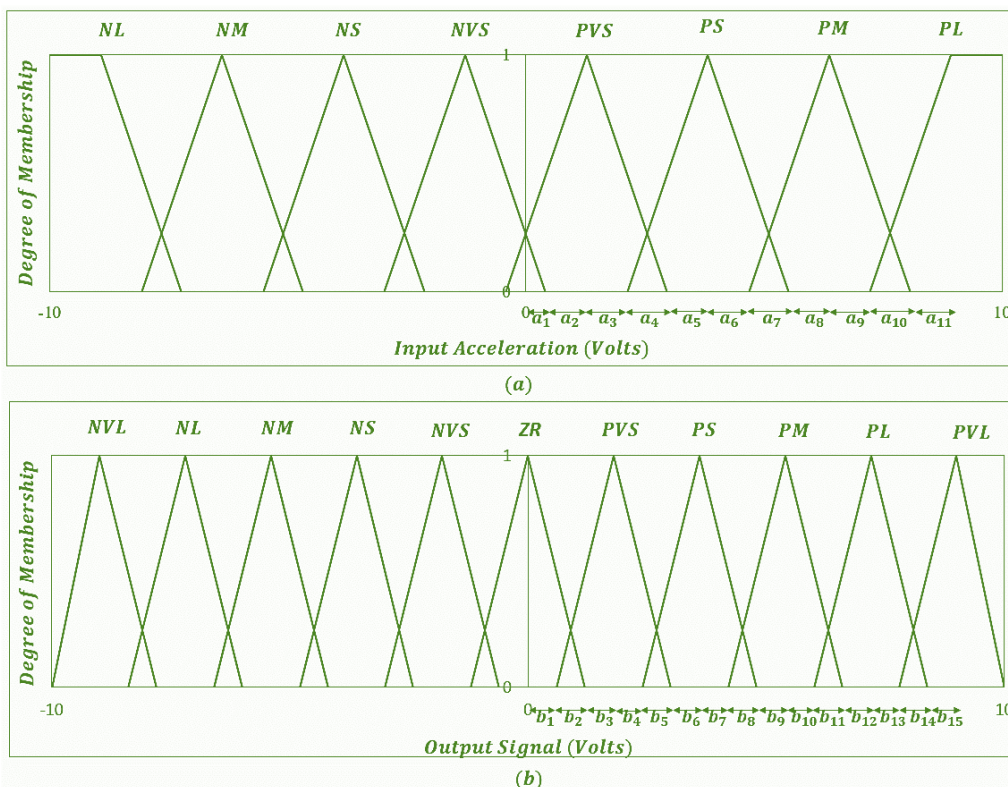


FIGURE 2. Membership functions for the input fuzzification (a) and the output defuzzification (b) with parametrically defined supports.

TABLE 2. The rule base of the FLC.

		Output Control Force						
		First acceleration input						
Second acceleration input	NL	NM	NS	NVS	PVS	PS	PM	PL
NL	PVL/c1	PL/c9	PM/c17	PS/c25	PVS/c33	ZR/c41	NVS/c49	NS/c57
NM	PL/c2	PM/c10	PS/c18	PS/c26	PVS/c34	ZR/c42	NVS/c50	NS/c58
NS	PM/c3	PS/c11	PS/c19	PVS/c27	PVS/c35	ZR/c43	NVS/c51	NS/c59
NVS	PM/c4	PS/c12	PVS/c20	PVS/c28	ZR/c36	NVS/c44	NS/c52	NM/c60
PVS	PM/c5	PS/c13	PVS/c21	ZR/c29	NVS/c37	NVS/c45	NS/c53	NM/c61
PS	PS/c6	PVS/c14	ZR/c22	NVS/c30	NVS/c38	NS/c46	NS/c54	NM/c62
PM	PS/c7	PVS/c15	ZR/c23	NVS/c31	NS/c39	NS/c47	NM/c55	NL/c63
PL	PS/c8	PVS/c16	ZR/c24	NVS/c32	NS/c40	NM/c48	NL/c56	NVL/c64

III. Grey wolf Optimizer (GWO)

A. The Standard GWO

The GWO is an iterative metaheuristic algorithm drawing inspiration from the hunting behavior and social hierarchy of grey wolves to solve optimization problems

[33]. In nature, grey wolves live and hunt in a pack. During hunting, the pack first identifies some moving prey, then it encircles the prey to trap it, and ultimately attacks the prey. The GWO utilizes a predefined number of search agents whose position in the search space is iteratively updated

with respect to the (unknown) position of the global optimum by mimicking the encircling behavior of individual grey wolves in a hunting pack around an identified moving prey. This behavior is mathematically modelled by firstly defining the distance between the position vector of a wolf (search agent), $\vec{X}^{(k)}$, and the position vector of prey, $\vec{X}_p^{(k)}$, at the k th iteration, by [33]

$$\vec{D} = \left| \vec{C} \cdot \vec{X}_p^{(k)} - \vec{X}^{(k)} \right| \quad (1)$$

where

$$\vec{C} = 2\vec{r}_1 \quad (2)$$

with \vec{r}_1 being a vector of random numbers uniformly distributed within [0,1]; and secondly updating the position of the wolf in the next iteration using

$$\vec{X}^{(k+1)} = \vec{X}_p^{(k)} - \vec{A} \cdot \vec{D} \quad (3)$$

where

$$\vec{A} = 2\vec{a} \cdot \vec{r}_2 - \vec{a} \quad (4)$$

with \vec{r}_2 being a vector of random numbers uniformly distributed within [0,1] and \vec{a} being a deterministically defined vector with equal and linearly decreasing elements over the course of iterations from 2 to zero.

To facilitate a geometric interpretation of Eqs.(1-4), Fig.3 depicts a grey wolf with current position $\vec{X}^{(k)} = (x, y)$ in a two dimensional space and several possible updated positions around some prey located at $\vec{X}_p^{(k)} = (x_p, y_p)$. Vectors \vec{r}_1 and \vec{r}_2 allow the wolf to update its position at any point around the prey for a given vector \vec{a} . For example, the updated position $\vec{X}^{(k+1)} = (x_p, y_p - y)$ can be reached for $\vec{a} = (1,1)$ by setting $\vec{r}_1 = (1,1)$ and $\vec{r}_2 = (0.5,1)$. Moreover, the randomness of vectors \vec{r}_1 and \vec{r}_2 whose values are different at each iteration and the monotonically reducing norm of vector \vec{a} with every iteration achieve efficient coupling of and smooth transition between exploration (ie, searching away from a local optimal solution, or prey, to find an improved solution, or better prey, elsewhere) and exploitation (ie, converging swiftly to the optimal solution once it is singled out, or attacking prey once it has been encircled) [33]. This can be appreciated by noting that for $|\vec{A}| < 1$ the updated position of the wolf will be closer to the prey and will eventually coincide for $|\vec{A}| = 0$, while for $|\vec{A}| > 1$ the wolf moves away from the prey which increases the chance of

identifying alternative, potentially better, prey. Due to the randomness of \vec{r}_2 , the value of $|\vec{A}|$ may increase or decrease in the next iteration, meaning that the search agent may “explore” moving away from a local optimal thus avoiding potential stagnation in a local solution or may “exploit” moving towards the identified solution. Importantly, the monotonic reduction of $|\vec{a}|$ in the course of iterations ensures that the probability that an agent exploits ($|\vec{A}| < 1$) in the next iteration rather than explores ($|\vec{A}| > 1$) increases as more iterations take place and that exploitation intensifies as $|\vec{A}|$ is more likely to take smaller values with $|\vec{a}|$ reducing in each iteration, ultimately reaching zero. Still, some level of exploration in the GWO is maintained even after several iterations through the random vector \vec{r}_1 or, equivalently, \vec{C} which models random hurdles that a wolf may face in approaching prey. This is manifested through a stochastic increase of the distance \vec{D} if $|\vec{C}| > 1$ in a subsequent iteration even though exploitation occurred (ie, ($|\vec{A}| < 1$)) in the current iteration. Thus, vector \vec{C} safeguards GWO from local optimal stagnation in the final iterations.

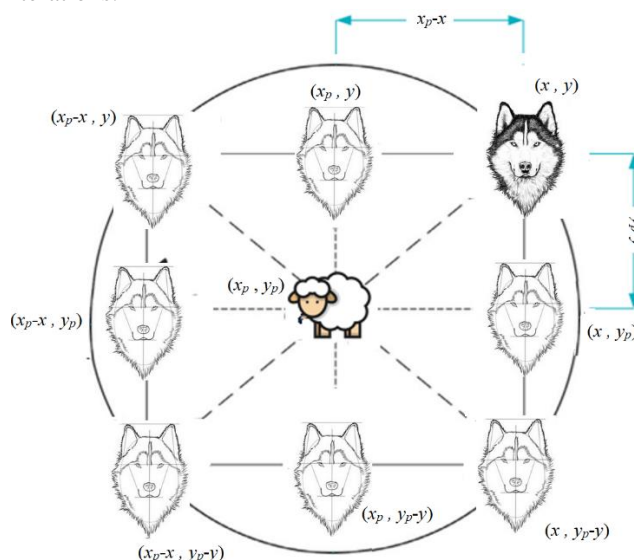


FIGURE 3. Position vectors of grey wolves and preys in two-dimensional space.

Further to the above considerations of randomness, exploitation, and exploration, which are important elements in all metaheuristic optimizers, the GWO benefits from a purposely unequal treatment of search agents in each iteration, reflecting the strict social ranking within any pack of grey wolves [33]. Specifically, every pack has a leader, the alpha (α) wolf who manages the pack and makes decisions, supported by a second in hierarchy deputy leader, the beta (β) wolf. Next in the hierarchy are the delta (δ) wolves who are delegated sensitive and important tasks for the pack including scouting and caretaking, and finally

the lowest ranked wolves are the omega (ω) who submit to all the other dominant wolves. The GWO assumes that there is one wolf from each of the three first rankings, α , β , and δ in the hunting pack who have better knowledge of the potential location of prey and the rest are all ω wolves who update their position following the three superior wolves. Thus, at the start of the k th iteration the three best solutions obtained thus far, $\vec{X}_\alpha^{(k)}$, $\vec{X}_\beta^{(k)}$ and $\vec{X}_\delta^{(k)}$ are selected based on the values of the objective function (fitness of solution) at the current location of all the agents and the position of all the agents are updated according to the location of the three best search agents, equally weighted. This is mathematically expressed, for the case of an arbitrary agent with position $\vec{X}^{(k)}$, by the set of equations [33]

$$\begin{cases} \vec{D}_\alpha = \left| \vec{C}_1 \cdot \vec{X}_\alpha^{(k)} - \vec{X}^{(k)} \right| \\ \vec{D}_\beta = \left| \vec{C}_2 \cdot \vec{X}_\beta^{(k)} - \vec{X}^{(k)} \right| \\ \vec{D}_\delta = \left| \vec{C}_3 \cdot \vec{X}_\delta^{(k)} - \vec{X}^{(k)} \right| \end{cases} \quad (5)$$

$$\begin{cases} \vec{X}_1 = \vec{X}_\alpha^{(k)} - \vec{A}_1 \cdot (\vec{D}_\alpha) \\ \vec{X}_2 = \vec{X}_\beta^{(k)} - \vec{A}_2 \cdot (\vec{D}_\beta) \\ \vec{X}_3 = \vec{X}_\delta^{(k)} - \vec{A}_3 \cdot (\vec{D}_\delta) \end{cases} \quad (6)$$

$$\vec{X}^{(k+1)} = \frac{\vec{X}_1 + \vec{X}_2 + \vec{X}_3}{3} \quad (7)$$

and graphically illustrated in Fig.4.

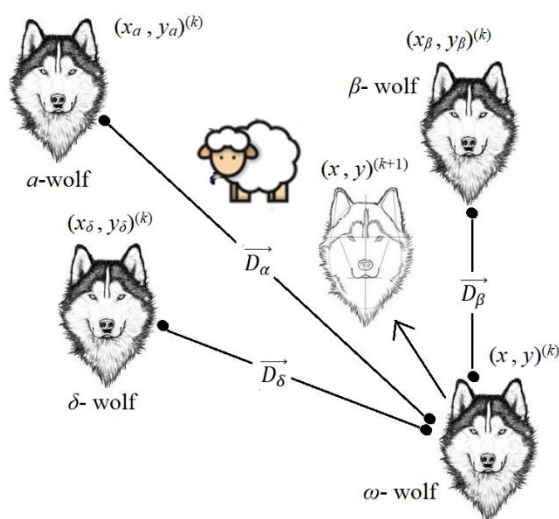


FIGURE 4. Illustration of updating the position of an ω wolf, based on the positions of the three best agents (α , β , δ wolves) with respect to the estimated position of prey in a two-dimensional space.

The pseudo code of the GWO is provided in Fig. 5 [33]. It is important to note that the use of the position of the three best agents by-passes the fact that the prey position (optimal global solution) is unknown, resulting in a feasible algorithm. It is further noted that the three best agents (dominant wolves) may not be the same in each iteration. The latter observation motivates a proposed improvement to the GWO algorithm detailed next.

```

procedure Grey Wolf Optimizer (GWO)
    Initialize the grey wolf population ( $X_i$ )
    Initialize  $a$ ,  $A$  and  $C$ 
    Calculate the fitness of each search agent
    Evaluate  $X_\alpha$  as the best search agent
    Evaluate  $X_\beta$  as the second best search agent
    Evaluate  $X_\delta$  as the third best search agent
    While  $t <$  maximum number of iterations
        for each search agent
            Update the position of the search agent by Eq. 7
        end for
        Update  $a$ ,  $A$  and  $C$ 
        Calculate the fitness of all search agents
        Update  $X_\alpha$ ,  $X_\beta$  and  $X_\delta$ 
    end while
end procedure
    
```

FIGURE 5. Pseudo code of the GWO [33].

B. The Upgraded Grey Wolf Optimizer (UGWO)

The standard GWO presented above takes a “discrete-time” or “iteration-time” approach in which the positions of the best three search agents are updated after the completion of each iteration. That is, after the position of all agents have been updated once. Whilst the discrete-time approach for evaluating the fitness of the achieved solution is followed by most of the standard metaheuristic algorithms, the evaluation of the fitness solution within each iteration may significantly benefit the quality of final best solution in problems with large population size. To this end, a “continuous-time” approach is herein proposed in which the fitness of solution is evaluated after each agent position is updated within an iteration. When applied to the GWO, the continuous-time approach allows for a potential change of the three best solutions within an iteration since an ω wolf may have moved closer to prey compared to the three dominant wolves. In this setting, the UGWO is reached which enables substitution of any one of three current best solutions within an iteration once (and if) it is surpassed by an agent who just updated its position. Then, the new set of best solutions is used to update the position of the remaining agents. The modified pseudo code of the UGWO based on the continuous-time approach is shown in Fig. 6.

```

procedure Upgraded Grey Wolf Optimizer (UGWO)
  Initialize the grey wolf population ( $X_i$ )
  Initialize  $a$ ,  $A$  and  $C$ 
  Calculate the fitness of each search agent
  Evaluate  $X\alpha$  as the best search agent
  Evaluate  $X\beta$  as the second best search agent
  Evaluate  $X\delta$  as the third best search agent
  While  $t <$  maximum number of iterations
    for each search agent
      Update the position of the search agent by Eq. 7
      Update  $a$ ,  $A$  and  $C$ 
      Calculate the fitness of all search agents
      Update  $X\alpha$ ,  $X\beta$  and  $X\delta$ 
    end for
  end while
end procedure
  
```

FIGURE 6. Pseudo code of the proposed UGWO.

IV. Benchmark Problem Description

A. Building Structure and Numerical Modelling

The proposed metaheuristic optimal FLC design approach is illustrated by application to a planar (two-dimensional) nonlinear computational model of a seismically excited 20-storey steel building equipped with an active control system. The structure is one of those considered in the third generation of seismic structural control benchmark problems [34]. The considered building, shown schematically in Fig.7, has been designed using a nominal design seismic action for the Los Angeles, CA, area with peak ground acceleration of 0.4g, $g=9.81\text{m/s}^2$ being the gravitational constant. It is 80.77m in height and 36.58m by 30.48m in plan. It includes two underground stories with 3.65m floor-to-floor height, while the ground floor is 5.49m in height and the rest of the floors are 3.96m in height. The seismic mass of the ground and the first levels are 5.32×10^5 kg and 5.63×10^5 , respectively, while for the second to 19th level, the seismic mass is 5.52×10^5 kg and for the 20th level is 5.84×10^5 kg.

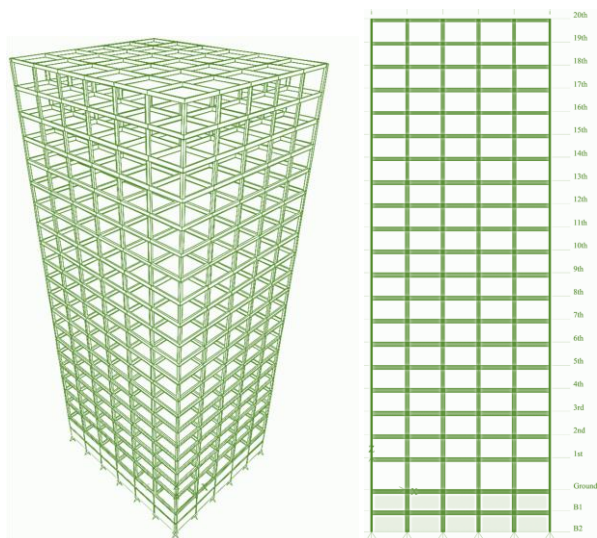


FIGURE 7. Twenty-story steel building (Left) and perimeter moment resisting frame along the weak direction (Right).

The lateral load resisting structural system of the building comprises four perimeter steel moment resisting frames (MRFs). The purpose of the seismic active control system is to protect the MRFs along the shorter (weak) direction of the building which has 5 bays spanning 6.10m each. Thus, a planar computational finite element model of one perimeter MRF, shown in Fig. 7, is considered in the numerical work. Details on material and section properties for all beams and columns of the considered MRF are presented in [34].

Under severe ground shaking, the considered steel MRF is expected to behave in a nonlinear fashion [34]. This is because modern seismic design codes for ordinary buildings, such as the one used to design the structure in Fig.7, allow for resisting seismic actions equal or above the nominal design seismic action through ductile inelastic behavior, which reduces upfront building construction costs [35]. For steel MRF buildings, this is achieved by ensuring material yielding at the ends of beams and columns with highest stress concentration resulting in the formation of flexural plastic hinges. These plastic hinges can dissipate significant input seismic (kinetic) energy without detrimental strength and stiffness degradation, thus without compromising the global structural stability. Herein, the anticipated inelastic material behavior under severe seismic action is mathematically represented by the bilinear hysteretic model in Fig.8, utilized in subsequent nonlinear time-domain analyses. The nonlinear model properties are defined in Table 3. The standard Newmark- β implicit direct time-integration method [36] is used for nonlinear structural analysis purposes, as detailed in [37] and hard-coded in MATLAB® as detailed in [38].

TABLE 3. Parameter specification of the nonlinear hysteresis model.

Properties	Value
Modulus of Elasticity	200,000 MPa
Yield Stress (σ_y)	345 MPa
Ultimate Stress (σ_u)	450 MPa
Yield Strain (ϵ_y)	0.001725
Ultimate Strain (ϵ_u)	0.018

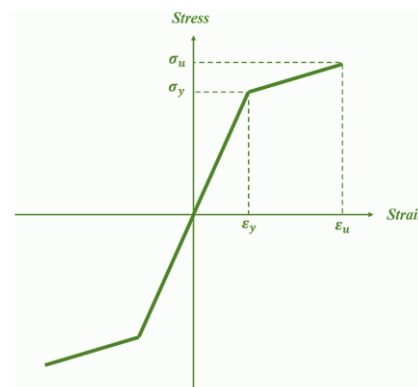


FIGURE 8. Bilinear material hysteresis model.

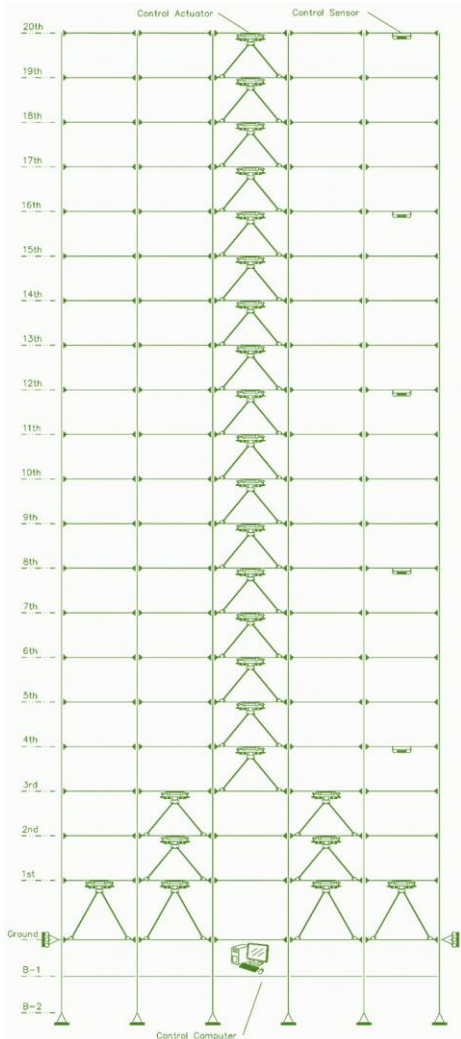


FIGURE 9. Active control system placement to the benchmark structure.

B. Active Control System

Whilst reducing upfront building costs, the main shortcoming of resisting severe earthquakes through nonlinear ductile material behavior is that it may incur significant monetary loss and reduced resilience in the event of major earthquakes [7]. This is because plastic hinges involve local structural damage which need to be repaired after an earthquake, alongside damage to non-structural elements, oftentimes at disproportionately high costs and downtime. To this end, the benchmark MRF is herein retrofitted by an active control system aiming to mitigate structural response to high intensity earthquakes, thus reducing the extend of nonlinear material behavior (plastic hinge formation). Following the benchmark active control problem in [34], active actuators are utilized to exert lateral control forces at different floors of the MRF. The maximum force capacity of each actuator is limited to 1000kN and a total of 25 actuators are provided to the MRF, with locations as seen in Fig. 9. A rigid chevron

brace is used to support each actuator as shown in Fig. 9, such that an actuator placed at the n -th floor produces equal and opposite forces exerted to the n and the $n+1$ floors. Five sensors acquiring lateral floor accelerations are implemented in the fourth, eighth, twelfth, sixteenth, and twentieth stories as seen in Fig.9. Four different FLCs defined in Section II are considered to provide the required control signals to the actuators, based on data streams from the sensors. Sensors in the 4th and 8th stories provide input to the first FLC which governs the control forces of the actuators in the first 8 stories. Sensors in 8th and 12th stories provide input to a second FLC which governs the control forces of the actuators located at 9th to 12th stories. Sensors in 12th and 16th stories provide input to a third FLC which governs the control forces of the actuators located at 13th to 16th stories. Lastly, sensors in 16th and 20th stories provide input to a fourth FLC which governs control forces of the actuators located at 17th to 20th stories. For numerical simulation, the considered benchmark seismic active control problem is implemented in SIMULINK® as illustrated in Fig. 10.

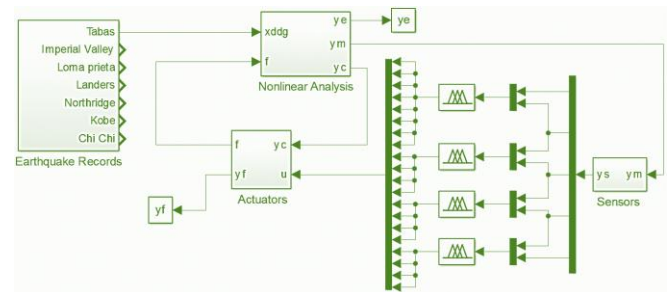


FIGURE 10. SIMULINK block diagram of the FLC-based active vibration control simulator of the 20-Story MRF building.

C. Seismic Input Action

In this paper, the efficacy of the benchmark active control problem in Fig. 9 to reduce earthquake-induced structural response and damage is numerically evaluated by considering 7 acceleration ground motion signals recorded during different major historic earthquake events with moment magnitude in the range of 6.6 to 7.6. Purposely, high-intensity near-fault ground motion records are chosen with epicentral distance in the range of 0.96km to 5.35km, to incur yielding (nonlinear response) to the benchmark structure. The number of records (7) is consistent with mandates of current building codes of practice for seismic design of structures [32]. Table 4 provides details of the events along with seismological characteristics and the absolute peak ground acceleration (PGA). The latter is the most used seismic intensity measure in earthquake engineering to characterize the damage potential of strong ground motions. It is seen that the considered records have $PGA \geq 0.65g$, which is significantly higher from the nominal

design $PGA=0.4g$ used in designing the 20-storey benchmark structure building [34]. It is therefore expected that the structure will behave nonlinearly (ie, some plastic

hinges will form at the ends of beams and columns) under the considered seismic records. The time histories of the chosen records are plotted in Fig. 11.

TABLE 4. Characteristics of the selected earthquake records.

Abbr.	Earthquake - Date	Moment magnitude	Epicentral distance (km)	Fault Mechanism	Station	Component	PGA (g)
EQ1	Tabas-1978	7.4	2.05	Reverse	TABAS	TABL1	0.854
EQ2	Imperial Valley-1979	6.6	2.66	Strike Slip	Bonds Corner	BCR230	0.777
EQ3	Loma Prieta-1989	6.9	3.85	Reverse Oblique	Corralitos	CLS000	0.645
EQ4	Landers-1992	7.3	2.19	Strike Slip	Lucerne	LCN345	0.789
EQ5	Northridge-1994	6.7	5.35	Reverse	Sylmar	SCS142	0.923
EQ6	Kobe-1995	6.9	0.96	Strike Slip	KJMA	KJM000	0.834
EQ7	Chi Chi-1999	7.6	3.12	Reverse Oblique	CHY028	CHY028N	0.760

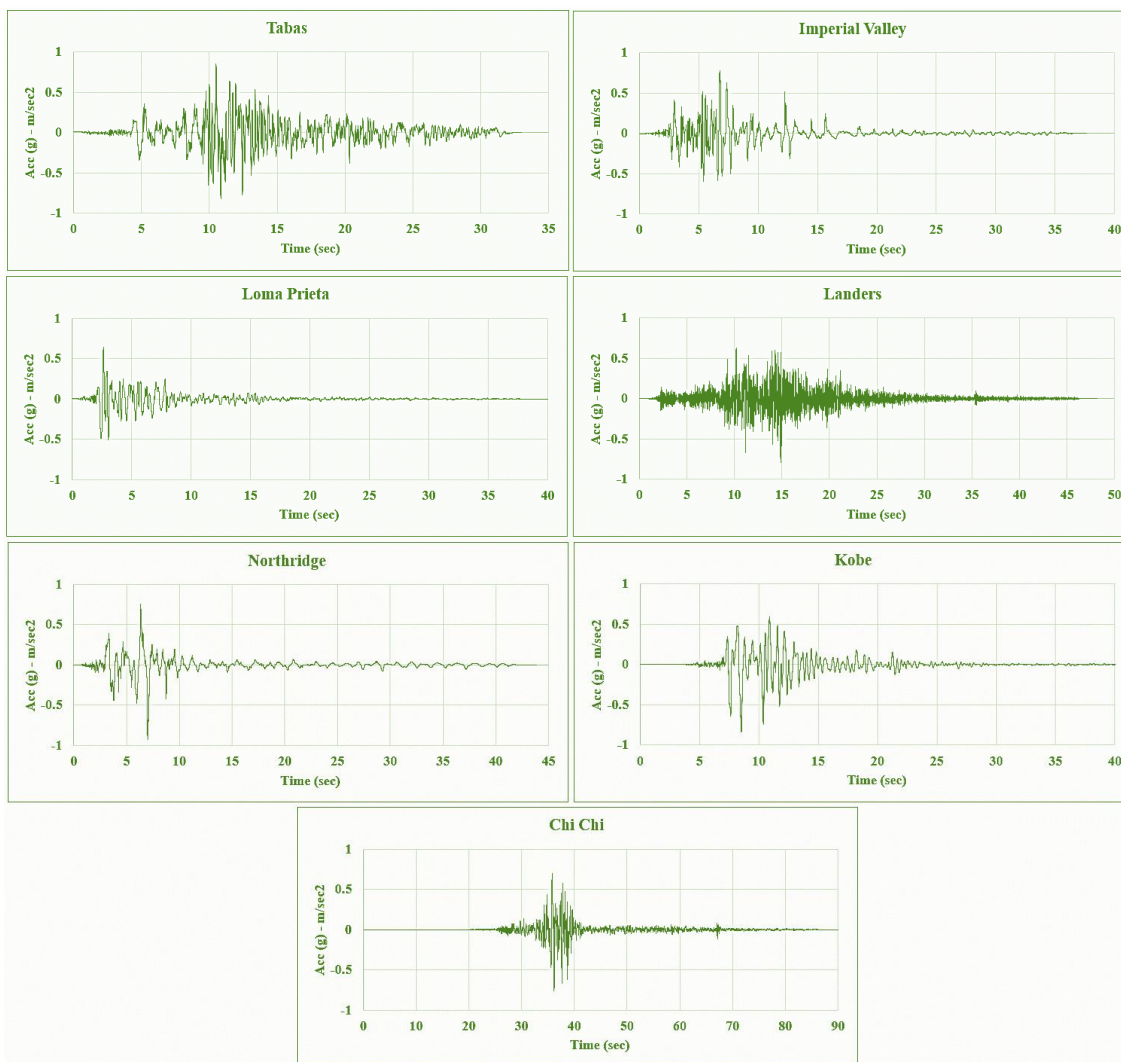


FIGURE 11. Acceleration time histories of the recorded seismic ground motion components in Table 4.

D. Performance Criteria

To assess the performance of the proposed metaheuristic optimal FLC design approach different performance criteria (PCs) for the actively controlled benchmark 20-storey structure are utilized. Following common practices [34], performance of the control system is gauged by comparing the response of the controlled structure to the response of the uncontrolled structure for the same earthquake excitation. In this regard, all PCs considered in this paper are ratios of some quantity of interest of the 20-storey MRF protected by the active control system with optimal FLC shown in Fig. 9 over the same or similar quantity for the 20-storey MRF with no control system in Figure 8. Thus, lower PC values correspond to better performance of the active control system.

The adopted PCs are divided into three categories, examining maximum in time structural response, level of peak structural damage (ie material yielding), and maximum in time requirements of the control system. The first category of PCs includes the maximum inter-story drift ratio (ie. relative peak displacement of two consecutive floors normalized by the floor height) of all stories, PC1, the maximum floor acceleration of all stories, PC2, and the maximum base shear (ie. sum of horizontal structural forces resisting lateral sway), PC3, developed from all 7 ground motions (EQ_s) of Table 4. Mathematically, these PCs are expressed as

$$PC_1 = \max_{7EQ_s} \left\{ \frac{\max_{t,i} \frac{|d_i(t)|}{h_i}}{\delta^{max}} \right\} \quad (8)$$

$$PC_2 = \max_{7EQ_s} \left\{ \frac{\max_{t,i} |\ddot{x}_{ai}(t)|}{\ddot{x}_a^{max}} \right\} \quad (9)$$

$$PC_3 = \max_{7EQ_s} \left\{ \frac{\max_{t,i} |\sum_i m_i \ddot{x}_{ai}(t)|}{F_b^{max}} \right\} \quad (10)$$

where $d_i(t)$ is the time-history of the inter-story drift ratio of the i th storey of the controlled structure, h_i is the i th storey height, δ^{max} is the peak inter-story drift ratio from all the stories of the uncontrolled structure, $\ddot{x}_{ai}(t)$ is the acceleration time-history of the i th floor of the controlled structure, \ddot{x}_a^{max} is the peak floor acceleration from all the floors of the uncontrolled structure, m_i is the seismic mass of the i th floor and F_b^{max} is the peak base shear of the uncontrolled structure.

The second category of PCs looks at the maximum ductility ratio (ie ratio of peak inelastic deformation over

yielding deformation), PC4, the maximum seismic energy dissipation at plastic hinges, PC5, and the number of plastic hinges, PC6. In the definition of PC4 and the PC5, the sum of the maximum curvature (ie, second derivative of the deflection) at both ends of structural members are taken. The mathematical expressions of PCs quantifying structural damage level are given as

$$PC_4 = \max_{7EQ_s} \left\{ \frac{\max_{t,j} \frac{|\varphi_j(t)|}{\varphi_{yj}}}{\varphi^{max}} \right\} \quad (11)$$

$$PC_5 = \max_{7EQ_s} \left\{ \frac{\max_{t,j} \frac{\int dE_j}{M_{yj} \cdot \varphi_{yj}}}{E^{max}} \right\} \quad (12)$$

$$PC_6 = \max_{7EQ_s} \left\{ \frac{N_d^c}{N_d} \right\} \quad (13)$$

where $\varphi_j(t)$ is the time-history of the curvature at the ends of the j th structural element in the controlled structure, φ_{yj} is the yield curvature at the ends of the j th structural element, φ^{max} is the maximum curvature over time across all the ends of structural members in the uncontrolled structure, $\int dE_j$ is the dissipated energy (ie, area of the bending moment versus curvature graphs) at the ends of the j th structural member in controlled structure, M_{yj} is the yield moment at the ends of the j th structural element, E^{max} is the maximum energy dissipated over time across all the ends of structural members in the uncontrolled structure, and N_d^c and N_d are the numbers of plastic hinges (damaged ends of structural members) in the controlled and in the uncontrolled structure, respectively.

The third category of PCs includes the maximum control force, PC7, the maximum stroke of the actuators (ie, relative displacement of the two device ends), PC8, and the maximum control power, PC9. The mathematical expressions of the last three PCs are given

$$PC_7 = \max_{7EQ_s} \left\{ \frac{\max_{t,k} |f_k(t)|}{W} \right\} \quad (14)$$

$$PC_8 = \max_{7EQ_s} \left\{ \frac{\max_{t,k} |y_k^a(t)|}{x^{max}} \right\} \quad (15)$$

$$PC_9 = \max_{7EQ_s} \left\{ \frac{\max_t |\sum P_l(t)|}{W \dot{x}^{max}} \right\} \quad (16)$$

where f_k , y_k^a , and P_k are the time-histories of the control force, stroke, and required power of the k th actuator, respectively, W is the MRF total weight, and x^{max} and \dot{x}^{max} are the maximum over time floor displacement and velocity relative to the ground of all floors of the uncontrolled structure.

V. Statement of the FLC Optimization Problem

For the purposes of this work, the parametrically defined FLC in section II is optimized to minimize structural damage of the controlled benchmark structure due to the seismic records in Table 4. To this end, the peak ductility ratio in terms of sum of the curvature at the end of structural members is taken as a most representative quantity of structural damage. This is closely related to PC4. However, for design purposes, PC4 is not used directly as the objective function to minimize as it does not account for the fact that records in Table 4 have different intensity and thus design would be dominated by the most severe record. Instead, a weighted sum approach is utilized in the definition of the objective function to minimize using the PGA of the records as weighting factors. This definition ensures that all records are accounted for in the FLC design independently of their intensity quantified by PGA. Mathematically, the objective function is written as

$$J = \frac{\sum_{i=1}^7 \left[PGA_i \times \max_i \left\{ \frac{\max_{t,j} \left| \frac{\varphi_j(t)}{\varphi_{y_j}} \right|}{\varphi_{max}} \right\} \right]}{\sum_{i=1}^7 PGA_i} \quad (17)$$

Thus, the FLC optimal design is formulated as follows: find the set of parameters defining the input fuzzification membership functions (a_1, a_2, \dots, a_{11} , in Fig. 2) for each of the two input streams, the output defuzzification membership functions (b_1, b_2, \dots, b_{15} , in Fig.2), and the fuzzy rule base (c_1, c_2, \dots, c_{64} , in Table 2), for the four FLCs of the benchmark problem such that the objective function in Eq.(17) is minimized. In this regime, there are 101 design variables for each FLC, thus a total of 404 design variables.

VI. Numerical Application

The fuzzy optimization problem detailed in the previous section is solved using the proposed UGWO, the standard GWO, as well as four other well-established in the literature metaheuristic optimization algorithms which have been used for FLC design applications as reviewed in the introduction, namely genetic algorithms (GA), particle swarm optimization (PSO), ant colony optimization (ACO), and imperialistic competitive algorithm (ICA). The same

stopping criteria are applied for all the algorithms, that is, 3000 objective function evaluations and 100 iterations. The efficacy of the algorithms to reach a meritorious FLC design for seismic active control in tall buildings is gauged by utilizing the PCs of the benchmark problem detailed in section IV.

The convergence history of the objective function in Eq.(17) for the six different algorithms under testing are presented in Fig. 12. It is seen that the UGWO finds the best solution from all considered algorithms. Specifically, it achieves a value of $J=0.8827$ for the objective function in Eq.(17), while the next best one is achieved by PSO ($J=0.9004$), followed by ICA ($J=0.9010$), GA ($J=0.9019$), GWO ($J=0.9042$), and ACO ($J=0.9124$). It is also seen that the UGWO converges in fewer iterations from all other algorithms except for ACO, which however yields the worst solution from all the considered algorithms and about 3.5% worse than the proposed UGWO. Through application of nonlinear time-domain analyses for the uncontrolled and the optimally FLC-based actively controlled benchmark structure, PCs in Eqs. (8-16) are derived for all six metaheuristic optimization algorithms considered.

Table 5 reports PCs obtained for each of the 7 ground motions in Table 4 for the proposed UGWO and the standard GWO. It also reports the difference of PC values achieved between the two algorithms with positive difference denoting improved performance of the proposed UGWO over the standard GWO. Besides the significant performance variability across different earthquake records, which is well-anticipated in structural earthquake engineering, it is seen that UGWO achieves better performance from the uncontrolled structure for all records for all PCs looking at peak structural responses (PC1-PC3) and level of inelastic response (PC4-PC6) indicative of structural damage, with only two exceptions highlighted in bold. Meanwhile, there are many more instances (13) for which the actively controlled structures using the standard GWO for FLC optimization performs worse than the uncontrolled structure. Moreover, with the exception of base shear PC3 for two records, the controlled structure with UGWO optimized FLC achieves improved performance than the GWO optimized FLC. The maximum improvements are up to 10.9% for PC1, 9.9% for PC2, 5.8% for PC3, 7.2% for PC4, 51.1% for PC5, and 11.8% for PC6, which are quite significant. Importantly, these improvements by using reduced peak control forces and actuator strokes by up 4.3% and 7.1%, respectively. At the same time, higher peak control power is required for 3 out of the 7 records for UGWO to achieve the improved performances compared to GWO. Overall, the reported data suggest an overall considerable improvement in seismic structural performance in using the UGWO over the GWO for the optimal FLC design.

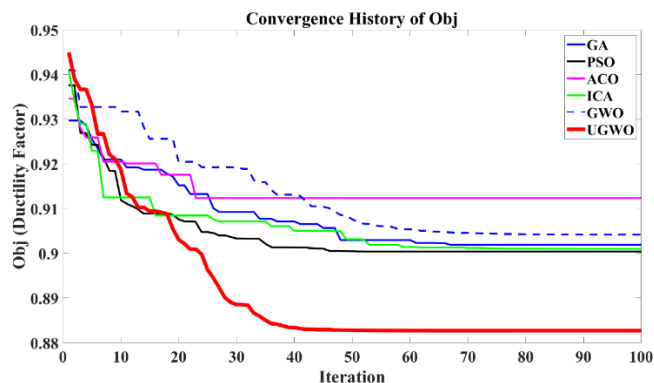


FIGURE 12. The convergence history of J objective function in Eq.(17) for the UGWO, GWO and four other metaheuristic optimization algorithms.

TABLE 5. Optimized evaluation criteria for the 20-story building utilizing UGWO.

Performance criteria	Optimization algorithm	Earthquake ground motions						
		EQ1	EQ2	EQ3	EQ4	EQ5	EQ6	EQ7
PC1 drift ratio	UGWO	0.967	0.879	0.937	0.993	0.891	0.871	0.997
	GWO	0.969	0.925	0.963	1.008	0.899	0.934	1.105
	difference	0.23%	5.23%	2.72%	1.60%	0.90%	7.14%	10.89%
PC2 Story Acceleration	UGWO	0.938	0.953	0.945	0.936	1.001	0.937	0.975
	GWO	0.951	0.972	0.956	1.029	1.006	0.960	1.034
	difference	1.39%	1.92%	1.16%	9.88%	0.44%	2.50%	6.05%
PC3 Base Shear	UGWO	1.045	0.773	0.801	0.954	0.937	0.880	0.771
	GWO	0.985	0.818	0.779	0.958	0.937	0.890	0.793
	difference	-5.70%	5.81%	-2.76%	0.36%	0.03%	1.23%	2.79%
PC4 Ductility	UGWO	0.927	0.827	0.919	0.996	0.858	0.800	0.862
	GWO	0.934	0.830	0.963	1.017	0.860	0.858	0.884
	difference	0.68%	0.25%	4.77%	2.19%	0.27%	7.21%	2.61%
PC5 Dissipated Energy	UGWO	0.904	0.302	0.430	0.992	0.969	0.924	0.998
	GWO	1.034	0.457	0.518	1.054	1.013	0.975	1.048
	difference	14.38%	51.14%	20.40%	6.23%	4.52%	5.51%	4.93%
PC6 Plastic Hinges	UGWO	0.920	0.708	0.606	1.000	0.985	1.000	0.949
	GWO	0.960	0.792	0.636	1.030	1.015	1.024	0.974
	difference	4.35%	11.77%	5.00%	3.03%	3.09%	2.38%	2.71%
PC7 Control Force	UGWO	0.0071	0.0071	0.0070	0.0071	0.0071	0.0071	0.0070
	GWO	0.0074	0.0073	0.0074	0.0071	0.0074	0.0074	0.0073
	difference	4.23%	2.82%	5.71%	0.00%	4.23%	4.23%	4.29%
PC8 Device Stroke	UGWO	0.090	0.180	0.167	0.096	0.180	0.137	0.122
	GWO	0.091	0.187	0.171	0.098	0.181	0.146	0.125
	difference	0.22%	3.44%	2.76%	1.56%	0.89%	7.10%	2.37%
PC9 Control Power	UGWO	0.008	0.012	0.010	0.007	0.010	0.011	0.012
	GWO	0.009	0.013	0.011	0.004	0.009	0.009	0.013
	difference	3.57%	12.17%	6.93%	-32.31%	-3.13%	-13.33%	8.94%

TABLE 6. Maximum PC from seven earthquake records obtained by different metaheuristic algorithms and difference with respect to the proposed UGWO.

Performance criteria	Metaheuristic algorithms					
	GA	PSO	ACO	ICA	GWO	UGWO
PC1	1.046	1.064	1.045	1.039	1.105	0.997
difference	4.98%	6.80%	4.87%	4.29%	10.89%	-
PC2	1.018	1.010	1.014	1.019	1.034	1.001
difference	1.61%	0.89%	1.27%	1.80%	3.30%	-
PC3	1.050	1.039	1.046	1.044	0.985	1.045
difference	0.46%	-0.52%	0.15%	-0.04%	-5.70%	-
PC4	0.991	1.002	0.998	0.998	1.017	0.996
difference	-0.48%	0.69%	0.20%	0.21%	2.19%	-
PC5	1.033	1.069	1.058	1.076	1.054	0.998
difference	3.44%	7.07%	6.00%	7.74%	5.53%	-
PC6	1.061	1.030	1.030	1.031	1.030	1.000
difference	6.06%	3.03%	3.03%	3.05%	3.03%	-
PC7	0.0075	0.0073	0.0072	0.0078	0.0074	0.0071
difference	5.63%	2.82%	1.41%	9.86%	4.23%	-
PC8	0.198	0.197	0.200	0.198	0.187	0.180
difference	9.71%	9.04%	11.09%	9.93%	3.44%	-
PC9	0.008	0.013	0.008	0.008	0.013	0.012
difference	-39.02%	3.25%	-37.40%	-36.59%	8.94%	-

Further numerical data are provided in Table 6 to enable a comparison of the performance of UGWO vis-à-vis all 5 alternative metaheuristic optimization algorithms considered in this work. Here, the peak PC value is reported from all seven records obtained by each algorithm together with percentage differences with respect to UGWO. With very few exceptions concerning mostly the base shear related performance (PC3) which is most relevant to strength issues rather than seismically induced damage, the UGWO achieves better seismic performance of the controlled benchmark structure than any other metaheuristic algorithm. Improvements are in the range of 4.3% to 10.9% and 3% to 6% for the all-important drift ratio (PC1) and number of plastic hinges (PC6), respectively, achieved by exerting reduced peak control forces by 1.41% up to 9.86% and exhibiting reduced peak actuator stroke by 3.44% up to 11.1%. This data establishes the superiority of the proposed UGWO over several previously used metaheuristic

algorithms for optimal FLC design in the rather challenging problem of seismic active control of tall buildings.

To gain further insights on the significance of the improved structural performance endowed by UGWO over GWO and over the uncontrolled structure, Figs. 13-15 present non-normalized data for the peak ductility ratio in terms of curvature and the peak energy dissipation ratio across all structural members of the benchmark structure, as well as the number of plastic hinges formed in the structure. Focusing first on the peak ductility ratio in Fig. 13, which is the most representative quantity of the level of highest damage in the structure, it is seen that UGWO achieves always improvement compared to the uncontrolled structure, even in cases where GWO does not improve performance. The maximum difference of the UGWO and GWO in comparison to the uncontrolled structure are for the Kobe earthquake record of about 20% and 17%, respectively.

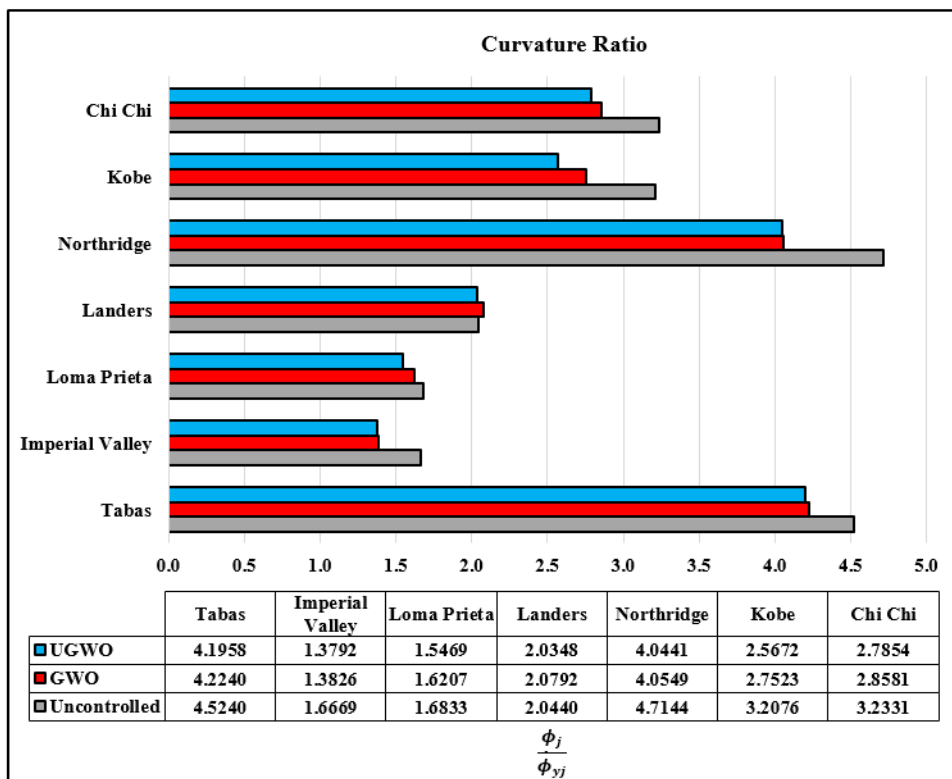


FIGURE 13. Comparison of the curvature ratio for different earthquakes.

Next, the attention is turned to the seismic energy dissipation ratio in Fig.14 whose reduced value is good indicator of the potentially positive effect of active control to resist earthquake shaking with reduced structural damage and thus reduced repair costs and downtime after a major seismic event. It is found that for all earthquakes the controlled benchmark structure optimized using the UGWO performs better from the uncontrolled, while this is not always the case with the GWO. Remarkably, for the imperial valley event, UGWO achieves 70% reduced energy dissipation through plastic deformation compared to only 54% achieved by the GWO.

Lastly, looking at Fig. 15, similar observations can be made for the number of plastic hinges (ie, locations of local structural damage), for which UGWO reduces the number of plastic hinges compared to the uncontrolled structures with the exception of Kobe and Landers seismic records for which the number of plastic hinges remain the same, though they slightly increase when using the GWO to optimize the FLC. Overall, despite record-to-record variability, the UGWO achieves always better performance than GWO which establishes the superiority of the best agent updating within each iteration of the GWO algorithm proposed in this paper.

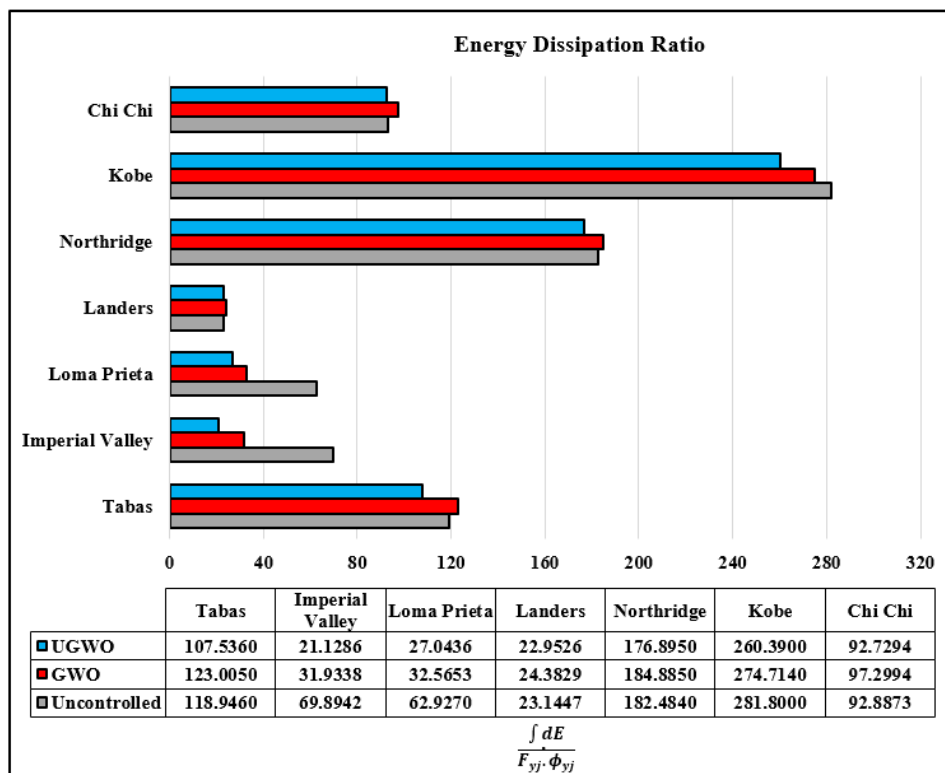


FIGURE 14. Comparison of the energy dissipation ratio for different earthquakes.

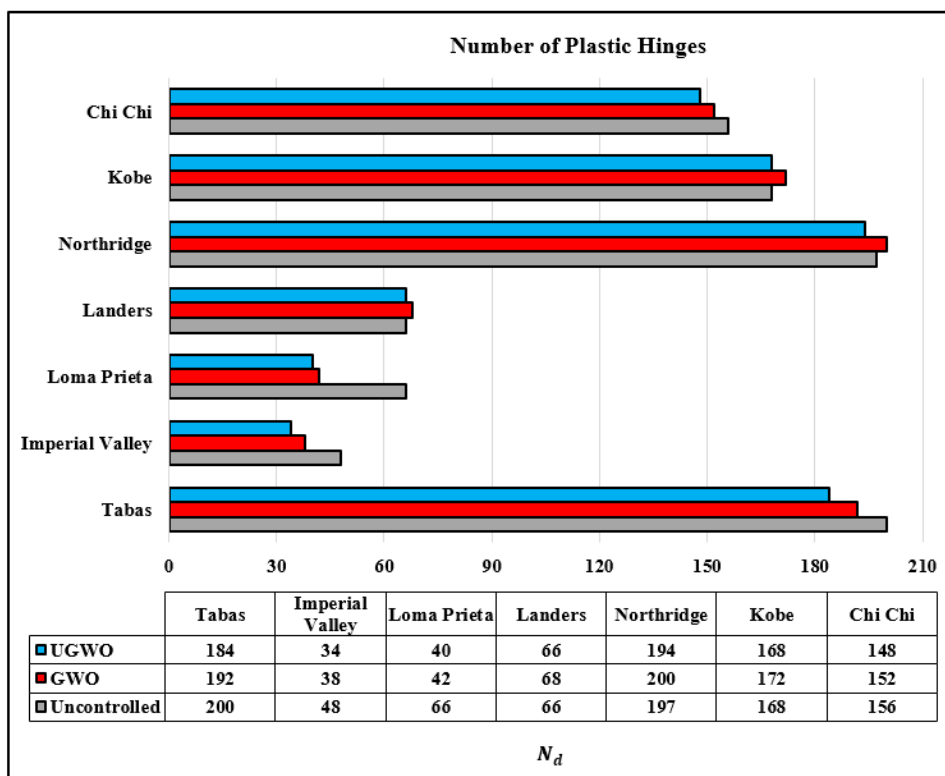


FIGURE 15. Comparison of the number of plastic hinges for different earthquakes.

VII. CONCLUDING REMARKS

In this paper, an enhanced version of the GWO algorithm has been proposed for the optimal design of FLCs aiming for seismic damage mitigation of tall buildings via active control. The efficacy of the proposed metaheuristic algorithm, UGWO, has been demonstrated by considering a benchmark 20-storey steel frame building actively controlled using 25 actuators. To this aim, a fuzzy optimal design problem has been considered involving 404 design variables tuned to minimize the inelastic response of the actively controlled benchmark structure for 7 high-intensity near fault recorded ground motions. It was found that FLC optimization using the proposed UGWO achieves reduced seismic demands for most of the ground motions compared to the uncontrolled structure, as well as compared to FLC-based actively controlled structure using GWO and four other metaheuristic optimization algorithms previously used in the literature for FLC optimal design. Seismic demands have been quantified in terms of six different performance indices including peak inter-storey drift, peak floor acceleration, peak ductility ratio, peak energy dissipation and number of plastic hinges developing. Further, the achieved higher reductions by the UGWO were accomplished using lower peak controlling force and peak actuator stroke. Overall, the reported numerical data establish the proposed UGWO as superior metaheuristic optimization algorithm for optimal FLC design and as a bona fide tool for reducing earthquake-induced damage to tall buildings under severe seismic events.

REFERENCES

- [1] MASNYC - The Municipal art Society of New York. *The Accidental Skyline 2017. Report MASNYC 2017. Available at <https://www.mas.org/pdf/accidental-skylinereport-10-15-2017-web.pdf>.*
- [2] Bilham R. *The seismic future of cities. Bulletin of earthquake engineering. 2009 Nov;7(4):839-87.*
- [3] Li Z, Adeli H. *Control methodologies for vibration control of smart civil and mechanical structures. Expert systems. 2018 Dec;35(6):e12354.*
- [4] Wen YK, Shinozuka M. *Cost-effectiveness in active structural control. Engineering structures. 1998 Mar 1;20(3):216-21.*
- [5] Allen RM, Melgar D. *Earthquake early warning: Advances, scientific challenges, and societal needs. Annual Review of Earth and Planetary Sciences. 2019 May 30;47:361-88.*
- [6] Gkoktsi K, Giaralis A. *A compressive MUSIC spectral approach for identification of closely-spaced structural natural frequencies and post-earthquake damage detection. Probabilistic Engineering Mechanics. 2020 Apr 1;60:103030.*
- [7] Freddi F, Galasso C, Cremen G, Dall'Asta A, Di Sarno L, Giaralis A, Gutiérrez-Urzúa F, Málaga-Chuquitaype C, Mitoulis SA, Petrone C, Sextos A. *INNOVATIONS in earthquake risk reduction for resilience: RECENT advances and challenges. International Journal of Disaster Risk Reduction. 2021 Apr 21:102267.*
- [8] Tse KT, Kwok KC, Tamura Y. *Performance and cost evaluation of a smart tuned mass damper for suppressing wind-induced lateral-torsional motion of tall structures. Journal of Structural Engineering. 2012 Apr 1;138(4):514-25.*
- [9] Petrini F, Giaralis A, Wang Z. *Optimal tuned mass-damper-inerter (TMDI) design in wind-excited tall buildings for occupants' comfort serviceability performance and energy harvesting. Engineering Structures. 2020 Feb 1;204:109904.*
- [10] Faravelli L, Yao T. *Use of adaptive networks in fuzzy control of civil structures. Computer-Aided Civil and Infrastructure Engineering. 1996 Jan;11(1):67-76.*
- [11] Tani A, Kawamura H, Seiko R. *Intelligent fuzzy optimal control of building structures. Engineering structures. 1998 Mar 1;20(3):184-92.*
- [12] Al-Dawod M, Samali B, Kwok K, Naghdy F. *Fuzzy controller for seismically excited nonlinear buildings. Journal of engineering mechanics. 2004;130(4):407-15.*
- [13] Ahlawat AS, Ramaswamy A. *Multi-objective optimal design of flc driven hybrid mass damper for seismically excited structures. Earthquake Engineering and Structural Dynamics. 2002; 31(7): 1459-1479.*
- [14] Reddy AS, Agarwal PK, Chand S. *Adaptive multipopulation genetic algorithm based self designed fuzzy logic controller for active magnetic bearing application. International journal of dynamics and control. 2018 Sep;6(3):1392-408.*
- [15] Hein D, Udluft S, Runkler TA. *Generating interpretable fuzzy controllers using particle swarm optimization and genetic programming. InProceedings of the Genetic and Evolutionary Computation Conference Companion 2018 Jul 6 (pp. 1268-1275).*
- [16] Vanishree J, Ramesh V. *Optimization of size and cost of static var compensator using dragonfly algorithm for voltage profile improvement in power transmission systems. International Journal of Renewable Energy Research (IJRER). 2018 Mar 11;8(1):56-66.*
- [17] Azizpanah-Abarghoee R, Malekpour M, Zare M, Terzija V. *A new inertia emulator and fuzzy-based LFC to support inertial and governor responses using Jaya algorithm. In2016 IEEE Power and Energy Society General Meeting (PESGM) 2016 Jul 17 (pp. 1-5). IEEE.*
- [18] Hasanpanah M, Amnieh HB, Khamesi H, Armaghani DJ, Golzar SB, Shahnazar A. *Prediction of an environmental issue of mine blasting: an imperialistic competitive algorithm-based fuzzy system. International Journal of Environmental Science and Technology. 2018 Mar;15(3):551-60.*
- [19] Boubertakh H. *Knowledge-based ant colony optimization method to design fuzzy proportional integral derivative controllers. Journal of Computer and Systems Sciences International. 2017 Jul;56(4):681-700.*
- [20] Caraveo C, Valdez F, Castillo O. *Optimization of fuzzy controller design using a new bee colony algorithm with fuzzy dynamic parameter adaptation. Applied Soft Computing. 2016 Jun 1;43:131-42.*
- [21] Sahoo DK, Sahu RK, Sekhar GC, Panda S. *A novel modified differential evolution algorithm optimized fuzzy proportional integral derivative controller for load frequency control with thyristor controlled series compensator. Journal of electrical systems and information technology. 2018 Dec 1;5(3):944-63.*
- [22] Debnath MK, Padhi JR, Satapathy P, Mallick RK. *Design of fuzzy-PID controller with derivative filter and its application using firefly algorithm to automatic generation control. In2017 6th International Conference on Computer Applications In Electrical Engineering-Recent Advances (CERA) 2017 Oct 5 (pp. 353-358). IEEE.*
- [23] Gheisarnjad M. *An effective hybrid harmony search and cuckoo optimization algorithm based fuzzy PID controller for load frequency control. Applied Soft Computing. 2018 Apr 1;65:121-38.*
- [24] Sahoo BP, Panda S. *Improved grey wolf optimization technique for fuzzy aided PID controller design for power system frequency control. Sustainable Energy, Grids and Networks. 2018 Dec 1;16:278-99.*
- [25] Zadeh MM, Bathaee SM. *Load frequency control in interconnected power system by nonlinear term and uncertainty considerations by using of harmony search optimization algorithm and fuzzy-neural network. InElectrical Engineering (ICEE), Iranian Conference on 2018 May 8 (pp. 1094-1100). IEEE.*
- [26] Olivas F, Valdez F, Melin P, Sombra A, Castillo O. *Interval type-2 fuzzy logic for dynamic parameter adaptation in a modified gravitational search algorithm. Information Sciences. 2019 Feb 1;476:159-75.*
- [27] Talatahari S, Motamedi P, Farahmand Azar B, Azizi M. *Tribe-charged system search for parameter configuration of nonlinear systems with large search domains. Engineering Optimization. 2021 Jan 2;53(1):18-31. <https://doi.org/10.1080/0305215X.2019.1696786>.*

- [28] Talatahari S, Azizi M. *Optimal design of real-size building structures using quantum-behaved developed swarm optimizer. The Structural Design of Tall and Special Buildings.* 2020 Apr 15; e1747. <https://doi.org/10.1002/tal.1747>.
- [29] Talatahari S, Azizi M, Toloo M. *Fuzzy Adaptive Charged System Search for global optimization. Applied Soft Computing.* 2021 May 24:107518.
- [30] Talatahari S, Azizi M. *Optimization of Constrained Mathematical and Engineering Design Problems Using Chaos Game Optimization. Computers & Industrial Engineering.* 2020 May 20:106560. <https://doi.org/10.1016/j.cie.2020.106560>
- [31] Azizi M. *Atomic orbital search: A novel metaheuristic algorithm. Applied Mathematical Modelling.* 2021 May 1;93:657-83. <https://doi.org/10.1016/j.apm.2020.12.021>
- [32] Azizi M, Talatahari S, Giaralis A. *Optimization of Engineering Design Problems Using Atomic Orbital Search Algorithm. IEEE Access.* 2021 Jul 12.
- [33] Mirjalili S, Mirjalili SM, Lewis A. *Grey wolf optimizer. Advances in engineering software.* 2014 Mar 1;69:46-61.
- [34] Ohtori Y, Christenson RE, Spencer Jr BF, Dyke SJ. *Benchmark control problems for seismically excited nonlinear buildings. J Eng Mech* 2004 Apr;130(4):366-85.
- [35] Avramidis I, Athanatopoulou A, Morfidis K, Sextos A and Giaralis A. *Eurocode-compliant seismic analysis and design of r/c buildings: Concepts, commentary and worked examples with flowcharts, Springer International Publishing, ISBN 978-3-319-25269-8, p. 488, 2016.*
- [36] Newmark NM. *A method of computation for structural dynamics. Journal of the engineering mechanics division.* 1959 Jul 3;85(3):67-94.
- [37] Subbaraj K, Dokainish MA. *A survey of direct time-integration methods in computational structural dynamics—II. Implicit methods. Computers & Structures.* 1989 Jan 1;32(6):1387-401.
- [38] Ohtori Y, Spencer Jr BF. *A MATLAB-based tool for nonlinear structural analysis. InProc. of the 13th Engineering Mechanics Conf 1999 Jun (pp. 13-16).*
- [39] Beyer K, Bommer JJ (2007) *Selection and scaling of real accelerograms for bi-directional loading: a review of current practice and code provisions. Journal of earthquake engineering* 11 (S1):13-45.